Autonomous Waypoint Transitioning and Loitering for Unmanned Aerial Vehicles via Hybrid Control

Dean W. Smith III* and Ricardo G. Sanfelice†

We consider the problem of autonomously controlling a fixed-wing aerial vehicle to visit a neighborhood of a pre-defined waypoint, and when nearby it, loiter around it. To solve this problem, we propose a hybrid feedback control strategy that unites two state-feedback controllers: a *global controller* capable of steering or transitioning the vehicle to nearby the waypoint and a *local controller* capable of steering the vehicle about a loitering radius. The aerial vehicle is modeled on a level flight plane with system performance characterized in terms of the aerodynamic, propulsion, and mass properties. Thrust and bank angle are the control inputs. Asymptotic stability properties of the individual control algorithms, which are designed using backstepping, as well as of the closed-loop system, which includes a hybrid algorithm uniting the two controllers, are established. In particular, for this application of hybrid feedback control, Lyapunov functions and hybrid systems theory are employed to establish stability properties of the set of points defining loitering. The analytical results are confirmed numerically by simulations.

Nomenclature

$\|x\|$	Euclidean norm of x
$\mathcal{A}$	Set to be stabilized
c	level set, constant
$\mathcal{C}$	Hybrid system flow set
C_D	Drag coefficient
C_{D0}	Zero lift drag coefficient
C_L	Lift coefficient
$\mathcal{D}$	Hybrid system jump set
D	Drag, N
e	Error function
f	Hybrid system flow map
G	Hybrid system jump map
g	Gravity, m/s^2
h	Altitude, m
$\mathcal{H}$	Hybrid system
k	Controller gain
K	Drag Polar Coefficient
$\mathcal{K}_\infty$	Family of continuous functions that are zero at zero, strictly increasing, and unbounded
L	Lift, N
p	Local switching variable
q	Controller index
r	Turn radius, m
R	Magnitude of position vector, m
$\mathbb{R}$	Real numbers
s	dummy variable
S_{ref}	Wing reference area m^2
T	Thrust, N
U	Domain of hybrid system
v	Airspeed, m/s
V	Lyapunov function
W	Weight, N
x	x position, m
y	y position, m
z	State vector of hybrid system
α	class κ_∞ function
κ	Controller
ρ	Air density, kg/m^3
μ	Local controller rotation hysteresis
Ψ	Heading, deg
Φ	Bank angle

Subscripts

0	Initial Condition
b	Body Frame
C	Commanded

I. Introduction

Autonomous navigation of unmanned aerial vehicles (UAVs) require algorithms that are capable of accurately controlling the motion of the vehicle with only limited control authority. Recent results in the literature demonstrate that feedback control algorithms can be designed to steer UAVs along different paths by "reshaping" the vector fields that describe the motion of the vehicle under the effect of a guidance law defined by a particular set of differential equations [1,2]. Paths defined by a closed curve are of most interest as they require the control algorithms to maintain

*Raytheon Missile Systems, Guidance Navigation and Control Center, Tucson, AZ
†University of California, Computer Engineering Department, Santa Cruz, CA

Approved for Public Release.
DoD OPSR 15-S-1455. May 2015.

the vehicle aloft along a recurrent path (not necessarily circular nor periodic), which is a key building block in almost every UAV mission as it can be efficiently employed as an intermediate "fly stage" to transition to a new location, perhaps by following a pre-planned straight or curved path[3].

An alternative to the vector field shaping technique mentioned above is to rely on multiple controllers, each of them designed to accomplish a different task, and appropriately switch among them. In such approach, a supervisory control algorithm monitors the state of the vehicle and, based on the given mission, determines which controller should be applied at each instant. The switching logic should be capable of "piecing together" the individual controllers to achieve the desired vehicle motion. While the approach allows independent design of the individual controllers, the emergence of discrete (or discontinuous) dynamics is unavoidable, which may make the analysis more involved (e.g., see the example in[4], which shows that two controllers – a local and a global continuous-time controller – cannot be united using a continuous-time supervisor). Fortunately, recent advances in the literature of hybrid systems have made systematic design of control algorithms piecing together individual controllers possible[5]. Interestingly, the design of such systems can be performed to yield a closed-loop system that is robust with respect to measurement noise, actuator errors, and external disturbances; see, e.g.,[6]. Due to these unique capabilities, the said hybrid systems approach to the combination of multiple controllers has been succesfully employed in different applications, such as the stabilization of an inverted pendulum[5] and of the position and orientation of a mobile robot[7]. Furthermore, the technique has been extended in[8] to allow for the combination of multi-objective controllers, including state-feedback laws as well as open-loop control laws. In the context of performance, a trajectory-based approach was also employed in[9] to generate dwell-time and hysteresis-based control strategies that guarantee an input-output stability property characterizing closed-loop system performance.

In this paper, we employ the switching/hybrid approach outlined above to provide a solution to the problem of autonomously controlling a fixed wing aerial vehicle to visit a neighborhood of a pre-defined waypoint, and when nearby it, loiter around it. More precisely, we propose a hybrid feedback control strategy that unites two state-feedback controllers: a *global controller* capable of steering or transitioning the vehicle to nearby the waypoint and a *local controller* capable of steering the vehicle about a loitering radius. Following[10], the aerial vehicle is modeled on a level flight plane with system performance characterized in terms of the aerodynamic, propulsion, and mass properties. The resulting model is nonlinear and with thrust and bank angle being its control inputs. This nonlinear UAV bank-to-turn model partially resembles a ship course controller model[11], where heading is controlled indirectly through the heading rate. For this vehicle model and employing Lyapunov stability theory, we established the asymptotic stability properties of the individual control algorithms designed. Both the local and global controllers are designed using the backstepping control design technique[12,13].

With the region of attraction induced by each controller being characterized, the closed-loop system incorporating a hybrid algorithm uniting the individual controllers is shown to be asymptotically stable using stability tools for hybrid systems. Finally, numerical results confirm the analytical findings.

The remainder of the paper is organized as follows. Section 2 presents a short description of the framework used for analysis including nomenclature for the hybrid system. The main result follows in Section 3. This section starts by introducing the problem to be solved, the proposed formulation of a solution, and the required assumptions. In addition to presenting a design procedure for the united control law, it establishes a robust stability property of the closed-loop system. In Section 4, the proposed control law is demonstrated in several simulations.

II. Problem Formulation

We consider the problem of stabilizing an aerial vehicle to a loiter around a given waypoint with specified velocity. Figure 1 depicts the scenario of problem to be solved, where v is the airspeed of the vehicle, $(x, y) \in R^2, 2s$ describe its position, and Ψ its heading angle. In this way, the vehicles velocity and heading angle are related by

$$v = \sqrt{\dot{x}^2 + \dot{y}^2}, \quad \Psi = \angle \left(\begin{bmatrix} \dot{x} \\ \dot{y} \end{bmatrix} \right), \tag{1}$$

where

$$\angle : \mathbb{R}^2, 2s \setminus \{0\} \rightrightarrows [-\pi, \pi] \tag{2}$$

defines the angle, positive in a clockwise direction, between the vector input and the positive vertical axis (x). Without loss of generality, the waypoint is assumed to be at the origin of the position coordinates (x, y) and the desired radius for loitering is R_C. Note that $\angle$ is undefined when x and y are 0. The forces on the UAV are described in the body frame (x_b, y_b) and can be transformed into the plane of the absolute frame (x, y) using the heading angle Ψ, via

$$\begin{bmatrix} \cos\Psi & -\sin\Psi \\ \sin\Psi & \cos\Psi \end{bmatrix} \tag{3}$$

Several assumptions are made in order to focus the analysis for the scope of this paper. These assumptions are listed below:

- UAV modeled as a point mass;
- Level flight in the (x, y) plane;
- Gravitational acceleration is constant;
- Aerodynamic properties modeled as a simple drag polar with a maximum lift coefficient;
- Propulsion performance is limited by a maximum thrust;
- Mass is constant (no fuel burn);
- Vehicle "banks" to turn and the bank angle Φ satisfies $\Phi \in \left(-\frac{\pi}{2}, \frac{\pi}{2}\right)$.

These assumptions are typical in the conceptual design phase of an aircraft where system level aerodynamic and propulsion performance are balanced to achieve mission objectives.

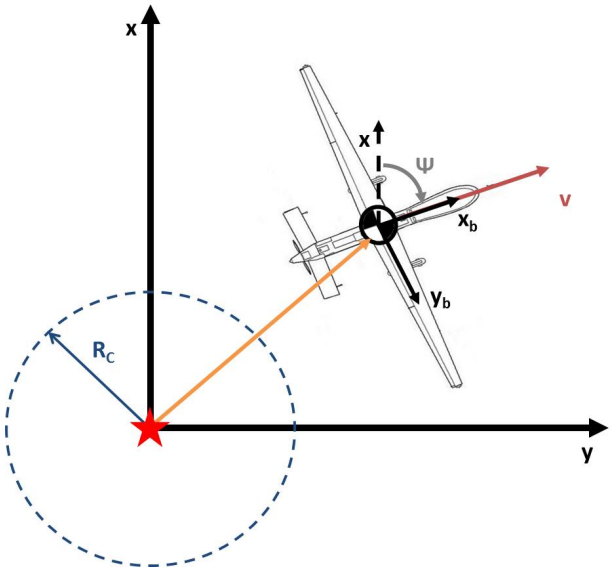

Figure 1. Waypoint Geometry.

A. Free Body Diagram

The equations of motion for the UAV are determined by using first principles. The free body diagram for the aircraft is shown in Fig. 2.

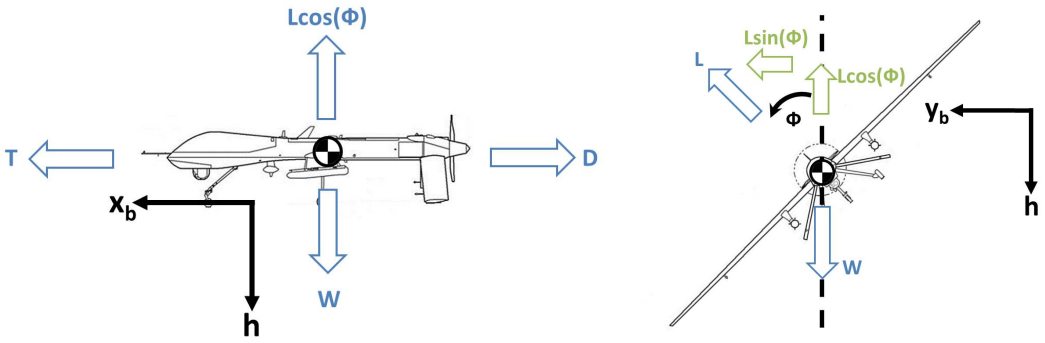

Figure 2. Level Flight Free Body Diagram.

Summing the forces in the body axes shown in Fig. 2 gives the equations

$$\sum F_{x_b} = T - D, \tag{4}$$

$$\sum F_{y_b} = L \sin \Phi, \tag{5}$$

$$\sum F_h = W - L \cos \Phi, \tag{6}$$

where T is thrust, D is drag, L is lift, W is weight, and Φ is bank angle. Since the problem is simplified to only consider motion in the plane, the sum of forces in the vertical direction in Eq. (6) are assumed to be equal to zero, which defines the lift required for the UAV to maintain altitude and is given by

$$\sum F_h = 0 \quad \Rightarrow \quad L = \frac{W}{\cos \Phi}. \tag{7}$$

B. Aerodynamic Model

Aerodynamic forces such as lift and drag are given by

$$L(v, \Phi) = C_L(v, \Phi) S_{ref} \frac{\rho v^2}{2}, \;\; D(v, \Phi) = C_D(v, \Phi) S_{ref} \frac{\rho v^2}{2}, \tag{8}$$

where lift and drag are expressed as coefficients (as defined in the nomenclature) and depend explicitly on the values of v and Φ. Substituting Eq. (8) into Eq. (7) allows one to solve for the required lift coefficient to balance the weight of the UAV, which is given by

$$C_L(v, \Phi) = \frac{2W}{S_{ref} \rho v^2 \cos \Phi}. \tag{9}$$

The drag coefficient (C_D) can be expanded into a zero lift drag component (C_{D0}) and an induced drag component as follows:

$$C_D(v, \Phi) = C_{D0} + K C_L(v, \Phi)^2. \tag{10}$$

Eq. (10) is known as a drag polar.[14]

C. State and Control Boundaries

The minimum speed and maximum bank angle of the UAV are limited by the maximum lift coefficient $C_{L\max}$. Explicit expressions for the minimum speed and maximum bank angle of a UAV obtained from Eq. (10) are given as follows:

$$v_{\min}(\Phi) = \sqrt{\frac{2W}{S_{ref} \rho C_{L\max} \cos \Phi}} \;\; \in \;\; \left[\sqrt{\frac{2W}{S_{ref} \rho C_{L\max}}}, \infty \right) \tag{11}$$

$$\Phi_{\max} = \cos^{-1}\left(\frac{2W}{S_{ref} \rho v^2 C_{L\max}} \right) \tag{12}$$

The maximum speed of the UAV is defined by the speed at which drag equals the maximum thrust $(T_{\max})$ of the UAV. Starting by setting the max thrust $T_{\max}$ equal to drag and substituting in the expressions for drag given in Eq. (10) and the expression for required lift given in Eq. (9) gives an algebraic expression involving velocity. Solving for velocity gives the maximum velocity

$$v_{\max} = \sqrt{\frac{T_{\max} + \sqrt{{T_{\max}}^2 - 16 C_{D0} W^2 K}}{\rho C_{D0}}}, \tag{13}$$

which occurs at a bank angle of zero.

D. Hybrid System Model

As outlined in Section I, our solution to the nonlinear control problem stated above consists of a hybrid feedback control strategy that unites two state-feedback controllers: a global controller capable of steering or transitioning the vehicle to nearby the waypoint and a local controller capable of steering the vehicle about a loitering radius. In this way, the closed-loop system resulting when applying our proposed hybrid control algorithm is a hybrid dynamical system. The state, which we denote by z, of the proposed aerial vehicle controlled by a hybrid control algorithm is given by

$$z = [x \;\; y \;\; v \;\; \Psi \;\; q]^\top \in U := \mathbb{R} \times \mathbb{R} \times [v_{\min}, v_{\max}] \times [-\pi, \pi] \times \{1, 2\} \tag{14}$$

where q is a switching variable that describes which controller is being utilized. A value $q = 2$ corresponds to the global (transit) controller and $q = 1$ corresponds to the local (loiter) controller being in the loop. The global controller will be designed to guide the vehicle at speed v_{C_2} to nearby the waypoint while the local controller will be designed to maneuver at a desired speed v_{C_1} about the loiter circle of radius R_C centered around the waypoint; see Figure 1. The parameter R_C defines the desired loiter circle radius used in the feedback law. The velocity is limited by the minimum and maximum steady level speed of the UAV ($v_{\min}$ and $v_{\max}$). For each $q \in \{1, 2\}$, the UAV's thrust (T_q) and bank angle (Φ_q) define the control inputs of the UAV and are constrained as follows:

$$(T_q, \Phi_q) \in [T_{\min}, T_{\max}] \times [-\Phi_{\max}, \Phi_{\max}]. \tag{15}$$

The switching between two controllers allows the dynamics of the UAV to be modeled as a hybrid system. The switch of controllers is a discrete event, while the motion of the UAV is a continuous flow of real time. The hybrid framework we employ in this work is presented in[5], where a generic hybrid system, $\mathcal{H}$, is given by four objects $(\mathcal{C}, f, \mathcal{D}, G)$ defining its data:

- Flow map: a single-valued map f defining the flows (or continuous evolution) of $\mathcal{H}$;
- Flow set: a set $\mathcal{C}$ specifying the points where flows are possible;
- Jump map: a set valued map G defining the jumps (or discrete evolution) of $\mathcal{H}$;
- Jump set: a set $\mathcal{D}$ specifying the points where flows are possible.

Then, for the control problem in this paper, a hybrid system $\mathcal{H} = (\mathcal{C}, f, \mathcal{D}, G)$ representing the closed-loop system from controlling the UAV using the transit and loiter controllers has state space U and can be written in the compact form

$$\mathcal{H}: \quad z \in U \quad \begin{cases} \dot{z} &= f(z, \kappa(z)) \quad z \in \mathcal{C} \\ z^+ &= G(z) \qquad z \in \mathcal{D} \end{cases}, \tag{16}$$

where κ is the feedback law applied to the control input of the UAV, which is given by

$$\kappa(z) = \kappa_q(z) = \begin{cases} \kappa_1(x, y, v, \Psi) & \text{if } q = 1 \text{ (local/loiter)} \\ \kappa_2(x, y, v, \Psi) & \text{if } q = 2 \text{ (global/transit).} \end{cases} \tag{17}$$

The flow and jump map for the UAV hybrid system are given by

$$f(z, (T_q, \Phi_q)) = \begin{bmatrix} v \cos \Psi \\ v \sin \Psi \\ \frac{T_q - D(v, \Phi_q)}{m} \\ \frac{g}{v} \tan \Phi_q \\ 0 \end{bmatrix} \tag{18}$$

$$G(z) = \begin{bmatrix} x \\ y \\ v \\ \Psi \\ 3 - q \end{bmatrix} \tag{19}$$

The flow map defines a differential equation that corresponds to the equations of motion for the UAV in the plane under the effect of the feedback law, as discussed previously, and the jump map toggles which controller is commanding thrust and bank angle. The events triggering jumps are determined by the following choice of the flow and jump sets:

$$\begin{aligned} \mathcal{C}_1 &:= \{z \in U : q = 1, |R(x, y) - R_C| \leq d, R(x, y) \neq 0\} \\ \mathcal{C}_2 &:= \left\{z \in U : q = 2, \frac{1}{2}\left((R(x, y) - R_C)^2 + (v - v_{C1})^2 + (\Psi - \Psi_{C1}(x, y))^2\right) \geq c, R(x, y) \neq 0\right\} \\ \mathcal{D}_1 &:= \{z \in U : q = 1, |R(x, y) - R_C| \geq d, R(x, y) \neq 0\} \\ \mathcal{D}_2 &:= \left\{z \in U : q = 2, \frac{1}{2}\left((R(x, y) - R_C)^2 + (v - v_{C1})^2 + (\Psi - \Psi_{C1}(x, y))^2\right) \leq c, R(x, y) \neq 0\right\} \end{aligned} \tag{20}$$

where $R(x, y) = \sqrt{x^2 + y^2}$ and [‡]

$$c > \frac{1}{2}\left(\pi^2 + (v_{\max} - v_{\min})^2\right) \tag{21}$$

$$d > \sqrt{2c}. \tag{22}$$

[‡]The flow and jump sets can be either a disk ($c \geq R_C$) or a donut ($c < R_C$) depending on the values selected for c and d.

The flow and jump sets were selected to ensure stability of the hybrid controller. This was done by ensuring that the boundary for the global jump set ($\mathcal{D}_1$) is contained in a sub-level set of the basin of attraction induced by the local controller. The details of this selection are discussed in the uniting global and local controller section, which is Section III.C. For the special case of $R = 0$, the hybrid system is undefined. However, solutions cannot remain at $R = 0$ because of the lower bound on velocity given in Eq. (25).

III. Design of Hybrid Controller for Transit and Loitering

The transit and loiter control laws for the UAV have different objectives. The transit control law will command a thrust to approach the loiter circle at transit velocity, while commanding a heading to point the UAV's velocity vector towards the loiter circle. In contrast, the loiter control law will command thrust (less than the maximum) to achieve the desired loiter velocity, while gradually commanding a heading to make the velocity vector of the UAV tangent to the desired loiter circle. Fig. 3 shows a block diagram of the closed-loop system where a hybrid controller performs the selection of transit and loiter mode.

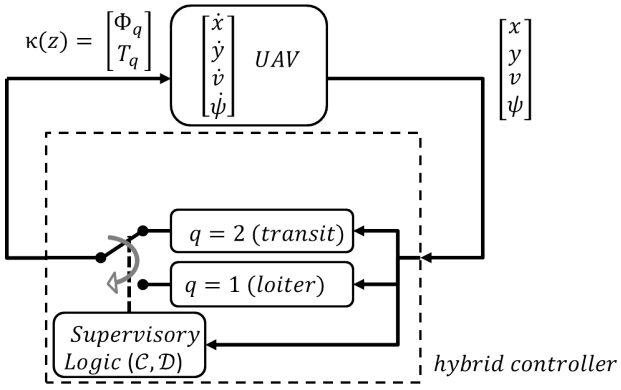

Figure 3. Control System Block Diagram.

The supervisory logic within the hybrid controller switches between the controllers to steer the UAV to the loiter circle and then loiter about it. The objective of the hybrid controller in loiter mode is to stabilize the UAV into a loiter pattern defined by a constant radius R_C and a constant velocity v_C, which implicitly defines a desired heading Ψ_C. The target set of points for the state components of the UAV (x, y, v, Ψ) and of the controller (q) is given by

$$\mathcal{A} = \{(x, y, v, \Psi, q) \in U : R(x, y) = R_C, v = v_{C_q}, \Psi = \Psi_{C_q}, q = 1\}. \tag{23}$$

Namely, the goal is to steer R to R_C at speed v_{C_q} with $q = 1$. For both the local and global controller, an error quantity for position, velocity, and heading angle will be defined. For each $q \in \{1, 2\}$ the error is given by

$$e_q = \begin{bmatrix} e_{1,q} \\ e_{2,q} \\ e_{3,q} \end{bmatrix} := \begin{bmatrix} R(x, y) - R_C \\ v - v_{C_q} \\ \Psi - \Psi_{C_q} \end{bmatrix}. \tag{24}$$

Asymptotic stability of the set $\mathcal{A}$ will be proven using the backstepping method[13] by first showing that the system can be stabilized by controlling Ψ directly. Section A covers the proof of stability for the loiter and transit controllers individually through Ψ actuation. Section B applies the backstepping method to the results from Section A to show that both the loiter and transit controllers can be stabilized individually with actuation through Φ. Section C combines the transit and loiter controllers from Section B to create a united hybrid controller that maintains the stability properties of the individual controllers.

A. Control design for the case of actuation through (T, Ψ)

In this case, the state of interest becomes

$$\tilde{z} = [x \;\; y \;\; v \;\; q]^\top \in \widetilde{U} := \mathbb{R} \times \mathbb{R} \times [v_{min}, v_{max}] \times \{1, 2\} \tag{25}$$

and the error system is defined as

$$\tilde{e}_q = \begin{bmatrix} \tilde{e}_{1,q} \\ \tilde{e}_{2,q} \end{bmatrix} := \begin{bmatrix} R(x, y) - R_C \\ v - v_{C_q} \end{bmatrix}. \tag{26}$$

The state error equation has continuous dynamics given by

$$\dot{\tilde{e}}_q = \begin{bmatrix} \frac{x}{R(x,y)} v\cos\Psi_q + \frac{y}{R(x,y)} v\sin\Psi_q \\ \frac{T_q - D(v)}{m} \end{bmatrix} \tag{27}$$

where the control input is defined as (T_q, Ψ_q). Note that in this case, drag is only a function of velocity $(i.e., D(v))$ instead of velocity and bank angle. A candidate Lyapunov function is given by

$$V_q(\tilde{e}_q) = \frac{1}{2}\tilde{e}_q^\top \tilde{e}_q. \tag{28}$$

Note that the target set of points from $\tilde{e}_q$ to stabilize is given by

$$\tilde{\mathcal{A}} = \{(x, y, v) : R(x, y) = R_C, v = v_{C_q}, q = 1\}, \tag{29}$$

and the flow and jump sets are defined as

$$\begin{aligned}
\tilde{\mathcal{C}}_1 &:= \left\{\tilde{z} \in \widetilde{U} : q = 1, |R(x,y) - R_C| \le \tilde{d}, R \neq 0\right\} \\
\tilde{\mathcal{C}}_2 &:= \left\{\tilde{z} \in \widetilde{U} : q = 2, \frac{1}{2}\left((R(x,y) - R_C)^2 + (v - v_{C1})^2\right) \ge \tilde{c}, R \neq 0\right\} \\
\tilde{\mathcal{D}}_1 &:= \left\{\tilde{z} \in \widetilde{U} : q = 1, |R(x,y) - R_C| \ge \tilde{d}, R \neq 0\right\} \\
\tilde{\mathcal{D}}_2 &:= \left\{\tilde{z} \in \widetilde{U} : q = 2, \frac{1}{2}\left((R(x,y) - R_C)^2 + (v - v_{C1})^2\right) \le \tilde{c}, R \neq 0\right\},
\end{aligned} \tag{30}$$

where

$$\tilde{c} > (v_{max} - v_{min})^2 \tag{31}$$

$$\tilde{d} > \sqrt{2\tilde{c}}. \tag{32}$$

The Lyapunov function given in Eq. (28) is lower and upper bounded by $\mathcal{K}_\infty$ functions defined as

$$\alpha_1(s) = \alpha_2(s) = \frac{1}{2}s^2 \text{ for each } s \ge 0. \tag{33}$$

Using Eq. (27), the variation of V_q with time can be expressed as

$$\left\langle \nabla V_q(\tilde{e}_q), \begin{bmatrix} \frac{x}{R(x,y)} v\cos\Psi_q + \frac{y}{R(x,y)} v\sin\Psi_q \\ \frac{T_q - D(v)}{m} \end{bmatrix} \right\rangle = \dot{R}(R(x,y) - R_C) + \frac{T_q - D(v)}{m}(v - v_{C_q}). \tag{34}$$

where $\dot{R}$ is the first entry of Eq. (27). The thrust control input affects the second term in Eq. (34). To ensure that this term is negative, a simple control law is one that guarantees that the thrust is larger than the drag if the current speed is smaller than the commanded speed, that is, $v - v_{C_q} < 0$, or smaller than the drag if the current speed is larger than the current commanded speed, that is, $v - v_{C_q} > 0$. When the desired speed is achieved, that is, $v = v_{C_q}$, the thrust can be set to be equal to the drag to maintain this speed. These properties are satisfied by proportional control law, that is,

$$T_q = D(v) - k_{T_q}(v - v_{C_q}), \tag{35}$$

where $k_{T_q} > 0$. It should be noted that though Eq. (35) applies to both the global and local regions, each region may have a different target velocity (v_{Cq}), effectively creating two different controllers. Plugging the expression for the commanded thrust in Eq. (35) into Eq. (34) leads to

$$\left\langle \nabla V_q(\tilde{e}_q), \begin{bmatrix} \frac{x}{R(x,y)} v\cos\Psi_q + \frac{y}{R(x,y)} v\sin\Psi_q \\ \frac{T_q - D(v)}{m} \end{bmatrix} \right\rangle = \dot{R}(R(x,y) - R_C) - \frac{k_{T_q}(v - v_{C_q})^2}{m}. \tag{36}$$

1. Global/Transit Controller (q=2)

The objective of the transit (global) controller $(q = 2)$ is to steer the UAV from every point in $\tilde{\mathcal{C}}_2$ to a point in $(\tilde{\mathcal{D}}_2)$ in finite time, so as to switch to the loiter (local) controller. In terms of the state variables, this means pointing the velocity vector of the UAV towards the loiter radius. The value of the commanded heading in the global region $(\tilde{\mathcal{C}}_2)$ is defined by the set-valued control law defined as

$$\Psi_{C_2}(x, y) = \angle\left(\begin{bmatrix} \bar{x} \\ \bar{y} \end{bmatrix}\right) \qquad \forall (x, y) \in \mathbb{R}^2 \text{ such that } \tilde{z} \in \tilde{\mathcal{C}}_2 \tag{37}$$

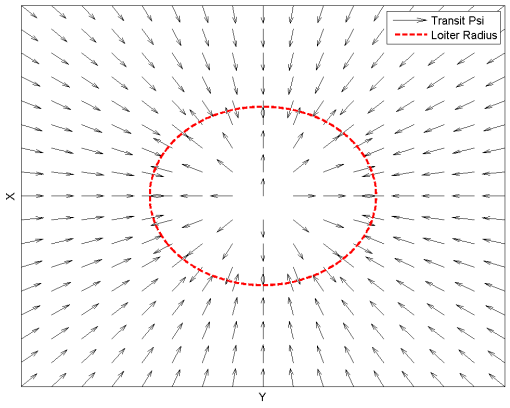

Figure 4. Quiver Plot of Global Controller Commanded Heading

where[§]

$$\bar{x} = \text{sign}(R_C - R(x,y))x$$
$$\bar{y} = \text{sign}(R_C - R(x,y))y$$

Note that the global heading controller is not defined on the loiter circle. This is because the local controller will be used in that region. Fig. 4 shows a quiver plot of the global controller heading with respect to a generic loiter circle. The direction of the arrows in the plot indicate the heading. The global controller commands a heading that is orthogonal and pointing towards the loiter circle.

Proposition 1 *For every function D, constant $m > 0$, velocity set-point $v_{C_2} \in [v_{\min}, v_{\max}]$, loiter radius $R_C > 0$, there exists $\gamma_2 \in \mathcal{K}_\infty$ such that the closed-loop system resulting from controlling the error system*

$$\dot{\tilde{e}}_2 = \begin{bmatrix} \frac{x}{R(x,y)} v \cos\Psi_2 + \frac{y}{R(x,y)} v \sin\Psi_2 \\ \frac{T_2 - D(v)}{m} \end{bmatrix},$$

with the controller

$$\begin{bmatrix} T_2 \\ \Psi_2 \end{bmatrix} = \tilde{\kappa}_2(x,y,v) := \begin{bmatrix} D(v) - k_{T_2}(v - v_{C_2}) \\ \Psi_{C_2}(x,y) \end{bmatrix}, \tag{38}$$

where $k_{T_2} > 0$ and Ψ_{C_2} is given in Eq. (37), is such that

1. $\left\langle \nabla V_2(\tilde{e}_2), \dot{\tilde{e}}_2 \right\rangle \leq -\gamma_2(|\tilde{e}_2|)$ *for all* $\tilde{e}_2 \in \mathbb{R}^2$ *such that* $[x\ y\ v\ 2]^\top \in \tilde{\mathcal{C}}_2$.
2. $|\dot{R}(x,y)| = v$ *for all* $[x\ y\ v\ 2]^\top \in \tilde{\mathcal{C}}_2$.

In particular, an appropriate choice for γ_2 is

$$\gamma_2(s) = \min\left\{ \frac{k_{T_2} s^2}{2m}, \frac{v_{min} s}{\sqrt{2}} \right\} \quad \forall s \geq 0.$$

2. *Local Controller*

The objective of the local controller $(q = 1)$ is to steer the state of the UAV to the desired loiter circle at the desired velocity. For the local controller, the set point velocity (v_{C_2}) used in Eq. (35) to determine the thrust input is the desired loiter speed. The expression for the local controller commanded heading shown in Eq. (40) is inspired by the control law in [1]. We incorporate a discrete dynamic parameter $p \in \{-1, 1\}$ designating the direction of rotation about

[§]The sign function returns +1 if the input is positive, -1 if the input is negative, and 0 if the input is 0.

the loiter circle. [¶] Then, the control law is defined by

$$\Psi_{C_1}(x,y) = \angle\left(\begin{bmatrix} y({R_C}^2 - R(x,y)^2) + p2xR(x,y)R_C \\ x({R_C}^2 - R(x,y)^2) - p2yR(x,y)R_C \end{bmatrix}\right) \forall (x,y) \in \mathbb{R}^2$$
$$\text{such that } \tilde{z} \in \tilde{\mathcal{C}}_1 \tag{40}$$

which is well-defined and single valued on $\tilde{\mathcal{C}}_1$. The local controller commands a heading that gradually approaches

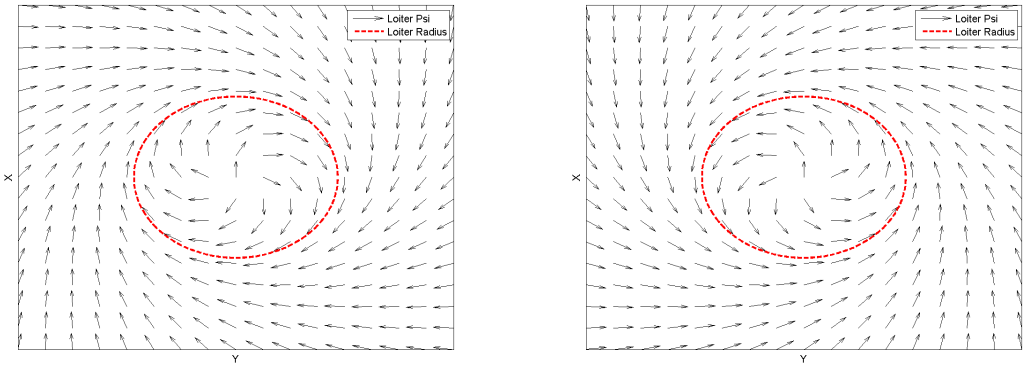

Figure 5. Quiver plot of local controller commanded heading (CW for p=1 and CCW for p=-1).

tangency with the loiter circle and settles on an equilibrium that can rotate clockwise or counter-clockwise depending on p. Selecting $p = -1$ gives a counter-clockwise rotation, and selecting $p = 1$ gives a clockwise rotation. Fig. 5 shows a quiver plot of the local controller heading with respect to a generic loiter circle. The direction of the arrows in the plot indicate the heading.

Proposition 2 *For every constant $m > 0$, velocity set-point $v_{C_1} \in [v_{\min}, v_{\max}]$, loiter radius $R_C > 0$, and parameter $p \in \{-1, 1\}$, there exists $\gamma_1 \in \mathcal{K}_\infty$ such that the closed-loop system resulting from controlling the error system*

$$\dot{\tilde{e}}_1 = \begin{bmatrix} \frac{x}{R(x,y)} v \cos\Psi_1 + \frac{y}{R(x,y)} v \sin\Psi_1 \\ \frac{T_1 - D(v)}{m} \end{bmatrix},$$

with the controller

$$\begin{bmatrix} T_1 \\ \Psi_1 \end{bmatrix} = \tilde{\kappa}_1(x,y,v) := \begin{bmatrix} D(v) - k_{T_1}(v - v_{C_1}) \\ \Psi_{C_1}(x,y) \end{bmatrix}, \tag{41}$$

where $k_{T_1} > 0$ and Ψ_{C_1} is given in Eq. (40), satisfies

$$\left\langle \nabla V_1(\tilde{e}_1), \dot{\tilde{e}}_1 \right\rangle \leq -\gamma_1(|\tilde{e}_1|) \quad \textit{for all} \quad \tilde{e}_1 \in \mathbb{R}^2 \textit{ such that } [x\ y\ v\ 1]^\top \in \tilde{\mathcal{C}}_1.$$

In particular, an appropriate choice for γ_1 is

$$\gamma_1(s) = \min\left\{ \frac{v_{min} R_C}{(R_C + \tilde{d})^2 + R_C^2}, \frac{k_{T_1}}{m} \right\} s^2 \qquad \forall\ s \geq 0,$$

Then, the origin of the local error coordinates ($\tilde{e}_1$) for the closed-loop system implementing the local controller on the flow set ($\tilde{\mathcal{C}}_1$) is asymptotically stable. Since the origin of $\tilde{e}_1$ corresponds to the points (x, y) in the loiter circle and loiter velocity equal to v_{C_q}, this also implies that the heading of the UAV on the loiter circle is tangent to the loiter circle as illustrated in Fig. 5.

The following result establishes that, for each $q \in \{1, 2\}$, the constraint $[T_{min}, T_{max}]$ is forward invariant under the feedback laws in (38) and (41) assigning T .

[¶]This parameter could become a state variable with discrete dynamics

$$p^+ = -p \quad \text{when} \quad \begin{cases} p = 1 \ \text{ and } \ \frac{1}{R(x,y)} \begin{bmatrix} x \\ y \end{bmatrix} \times \begin{bmatrix} \cos\Psi \\ \sin\Psi \end{bmatrix} \leq -\mu \\ p = -1 \ \text{ and } \ \frac{1}{R(x,y)} \begin{bmatrix} x \\ y \end{bmatrix} \times \begin{bmatrix} \cos\Psi \\ \sin\Psi \end{bmatrix} \geq \mu \end{cases} \tag{39}$$

and continuous dynamics $\dot{p} = 0$ where $\mu \in [0, 1]$ is a constant parameter that defines hysteresis for switching the value of p. The local controller is hybrid because of the switching of p. Switching is based on the cross product of unit position and velocity vectors as shown in Eq. (39). The selection of rotation direction in Eq. (39) utilizes the pre-existing rotation of the UAV around the loiter point based on the cross-product of the UAV's initial position and velocity vectors.

Lemma 1 *Under the effect of (35), $\tilde{e}_{2,q}$ evolves according to*

$$\dot{\tilde{e}}_{2,q} = -\frac{k_{T_q}}{m}\tilde{e}_{2,q}$$

and, since $\frac{k_{T_q}}{m} > 0$, we have that $\tilde{e}_{2,q} = 0$ is globally asymptotically stable. Furthermore, every solution to this subsystem with $T_q(0) \in [T_{min}, T_{max}]$ is such that

$$T_q(t) \in [T_{min}, T_{max}] \qquad \forall t \geq 0. \tag{42}$$

Remark The stability property of the origin (for $\tilde{e}_{2,q}$) follows directly from the resulting dynamics of $\tilde{e}_{2,q}$, which are obtained by plugging (35) into $\dot{\tilde{e}}_{2,q}$. In fact, under such feedback,

$$\tilde{e}_{2,q}(t) = \tilde{e}_{2,q}(0)e^{-\frac{k_{T_q}}{m}t} \qquad \forall t \geq 0 \tag{43}$$

for any initial condition $\tilde{e}_{2,q}(0)$. The property in (42) is a consequence of the resulting form of T in (35), since the substitution of (43) into (35) gives

$$T = D(v) - \tilde{e}_{2,q}(0)e^{-\frac{k_{T_q}}{m}t} \tag{44}$$

where if $T_q(0) \in [T_{min}, T_{max}]$, then $T_q(t) \in [T_{min}, T_{max}] \ \ \forall t \geq 0$.

B. Control design for the case of actuation through (T, Φ) via backstepping

The results in the previous section establish properties of the UAV when Ψ is a control input. However, for the hybrid system with flow map given in Eq. (18), Ψ is a function of the control input Φ. Using the method of backstepping, asymptotic stability will be proved for the hybrid system with Φ as a control input. Recall the error system given in Eq. (27) and add and subtract the desired heading Ψ_{Cq} from the heading state Ψ

$$\dot{e}_q = \begin{bmatrix} \frac{x}{R(x,y)}v\cos\left(\Psi - \Psi_{C_q} + \Psi_{C_q}\right) + \frac{y}{R(x,y)}v\sin\left(\Psi - \Psi_{C_q} + \Psi_{C_q}\right) \\ \frac{T_q - D(v,\Phi)}{m} \end{bmatrix}.$$

Now recall $e_{3,q}$ from Eq. (24) as the difference between the current heading Ψ and the commanded heading Ψ_{C_q} and evaluate its derivative, that is,

$$\begin{aligned} e_{3,q} &= \Psi - \Psi_{C_q} \\ \dot{e}_{3,q} &= \dot{\Psi} - \left\langle \nabla_z \Psi_{C_q}(z), f(z, \kappa(z)) \right\rangle, \end{aligned}$$

where, according to Eq. (18),

$$\dot{\Psi} = \frac{g}{v}\tan\Phi_q.$$

The dynamics of e_q are then

$$\dot{e}_q = \begin{bmatrix} \frac{x}{R(x,y)}v\cos\left(e_{3,q} + \Psi_{C_q}\right) + \frac{y}{R(x,y)}v\sin\left(e_{3,q} + \Psi_{C_q}\right) \\ \frac{T_q - D(v,\Phi)}{m} \\ \frac{g}{v}\tan\Phi_q - \left\langle \nabla_z \Psi_{C_q}(z), f(z, \kappa(z)) \right\rangle \end{bmatrix}. \tag{45}$$

Using

$$V_q(e_q) = V_q(\tilde{e}_q) + \frac{1}{2}{e_{3,q}}^2$$

for a Lyapunov function candidate, the derivative can be expressed as

$$\begin{aligned} \langle \nabla V_q(e_q), \dot{e}_q \rangle &= \left(\frac{x}{R}v\cos\left(e_{3,q} + \Psi_{C_q}\right) + \frac{y}{R}v\sin\left(e_{3,q} + \Psi_{C_q}\right)\right)(R - R_C) - \frac{k_{T_q}(v - v_{C_q})^2}{m} \\ &\quad + e_{3,q}\left(\frac{g}{v}\tan\Phi_q - \left\langle \nabla_z \Psi_{C_q}(z), f(z, \kappa(z)) \right\rangle\right) \\ \langle \nabla V_q(e_q), \dot{e}_q \rangle &= \left(\frac{x}{R(x,y)}v\left(\cos e_{3,q}\cos\Psi_{C_q} - \sin e_{3,q}\sin\Psi_{C_q}\right) + \frac{y}{R(x,y)}v\left(\sin e_{3,q}\cos\Psi_{C_q} + \cos e_{3,q}\sin\Psi_{C_q}\right)\right) \\ &\quad \times (R(x,y) - R_C) - \frac{k_{T_q}(v - v_{C_q})^2}{m} + e_{3,q}\left(\frac{g}{v}\tan\Phi_q - \left\langle \nabla_z \Psi_{C_q}(z), f(z, \kappa(z)) \right\rangle\right) \end{aligned} \tag{46}$$

From here, the control input Φ_q can be formulated for the specific global and local controllers to make the origin asymptotically stable for the system in Eq. (45) on the set $U \setminus \{z : R(x,y) = 0\}$.

1. Global Controller Backstepping

The global controller is designed to make the origin of the error system e_q asymptotically stable. This is achieved by inverting the tangent function containing Φ_2, the control input, and compensating for positive terms that come when differentiating the Lyapunov function. This results in the controller

$$\begin{aligned}
&\Phi_{C_2}(x, y, v, \Psi, e_{3,2}) \\
&\quad = \tan^{-1}\left(-\frac{k_{\Phi_2}(x, y, v, e_{3,2})ve_{3,2}}{g} + \frac{v}{g}\left\langle \nabla_z \Psi_{C_2}(z), f(z, \kappa_2(x, y, v, \Psi))\right\rangle\right) \\
&\quad = \tan^{-1}\left(-\frac{k_{\Phi_2}(x, y, v, e_{3,2})ve_{3,2}}{g} - \frac{yv^2}{gR(x, y)^2}\cos\Psi + \frac{xv^2}{gR(x, y)^2}\sin\Psi\right),
\end{aligned} \tag{47}$$

where the function k_{Φ_2} is of the form

$$k_{\Phi_2}(x, y, v, e_{3,2}) = \nu + \xi(e_{3,2})v|R(x, y) - R_C|, \tag{48}$$

$\nu > 0$, and $s \mapsto \xi(s)$ such that for each $s \in \mathbb{R}$

$$\xi(s) > \frac{1}{2} \text{ if } |s| \geq \frac{\pi}{2} \text{ and } \xi(s) \geq 0 \text{ if } |s| < \frac{\pi}{2}. \tag{49}$$

With the proposed definition of the function ξ we have that there exists $\beta \in (0, 1)\ s.t.\ \cos s + \xi s^2 \geq \beta$. Making the gain k_{Φ_2} a function of the system state allows for additional compensation for terms that arise when differentiating the Lyapunov function. Different values of ν and ξ can be selected, still satisfying the constraints in Eq. (49), as $e_{3,2}$ approaches zero, to prevent chattering of the controller commands.

Proposition 3 *For every constant $m > 0$, velocity set-point $v_{C_2} \in [v_{\min}, v_{\max}]$, and loiter radius $R_C > 0$, there exists $\gamma_2 \in \mathcal{K}_\infty$ such that the closed-loop system resulting from controlling the error system*

$$\dot{e}_2 = \begin{bmatrix} \frac{x}{R(x,y)}v\cos\left(e_{3,2} + \Psi_{C_2}\right) + \frac{y}{R(x,y)}v\sin\left(e_{3,2} + \Psi_{C_2}\right) \\ \frac{T_2 - D(v,\Phi)}{m} \\ \frac{g}{v}\tan\Phi_2 - \langle \nabla_z \Psi_{C_2}(z), f(z, \kappa_2(z))\rangle \end{bmatrix}, \tag{50}$$

with the controller

$$\begin{bmatrix} T_2 \\ \Phi_2 \end{bmatrix} = \kappa_2(x, y, v, \Psi, \Psi_{C_2}) := \begin{bmatrix} D(v, \Phi) - k_{T_2}(v - v_{C_2}) \\ \Phi_{C_2}(x, y, v, \Psi, e_{3,2}) \end{bmatrix}, \tag{51}$$

where $k_{T_2} > 0$, Ψ_{C_2} is given in Eq. (37), and Φ_{C_2} is given in Eq. (47), satisfies

1. $\langle \nabla V_2(e_2), \dot{e}_2\rangle \leq -\gamma_2(|e_2|)$ *for all* $e_2 \in \mathbb{R}^3$ *such that* $[x\ y\ v\ \Psi]^\top \in \mathcal{C}_2$

In particular, an appropriate choice of γ_2 is

$$\gamma_2(s) = \min\left\{\frac{v_{min}\beta s}{\sqrt{3}}, \frac{k_{T_2}s^2}{3m}, \frac{\nu s^2}{3}\right\}\ \forall s \geq 0.$$

2. Local Controller Backstepping

Similar to the global controller, the local controller is designed to make the origin of the error system asymptotically stable. This is achieved by inverting the tangent function containing Φ_1, the control input, and compensating for positive terms that come when differentiating the Lyapunov function. In this way the proposed controller is given by

$$\begin{aligned}
\Phi_{C_1}(x, y, \Psi, \Psi_{C_1}) &= \tan^{-1}\left[-\frac{k_{\Phi_1}(x, y, v, \Psi, \Psi_{C_1})ve_{3,1}}{g} + \frac{v}{g}\left\langle \nabla_z \Psi_{C_1}(z), f(z, \kappa_1(z))\right\rangle\right] \\
&= \tan^{-1}\left[-\frac{k_{\Phi_1}(x, y, v, \Psi, \Psi_{C_1})ve_{3,1}}{g} - \frac{yv^2}{gR(x, y)^2}\cos\Psi + \frac{xv^2}{gR(x, y)^2}\sin\Psi\right]
\end{aligned} \tag{52}$$

where k_{Φ_1} is given by

$$k_{\Phi_1}(x, y, v, \Psi, \Psi_{C_1}) = \chi + \gamma(e_{3,1})v\frac{(R_C + R(x, y))(R(x, y) - R_C)^2}{R_C^2 + R(x, y)^2} + \frac{|\sin e_{3,1}|}{\zeta^2}v2R(x, y)R_C|p|\frac{|R(x, y) - R_C|}{R_C^2 + R(x, y)^2} \tag{53}$$

where $\chi > 0$, $\zeta \in (0, \frac{\pi}{2})$ and $s \mapsto \gamma(s)$ is a smooth function such that

$$\gamma(s) > \frac{1}{2} \text{ if } |s| \geq \frac{\pi}{2}, \text{ and } \gamma(s) \geq 0 \text{ if } |s| < \frac{\pi}{2}. \tag{54}$$

With the proposed definition of the function γ we have that there exists $\beta \in (0, 1)\ s.t.\ \cos s + \gamma(s)s^2 \geq \beta\ \forall s \geq 0$. Note that making the "gain" k_{Φ_1} a function of the system's state allows for additional compensation of terms that arise when differentiating the Lyapunov function.

Proposition 4 *For every constant $m > 0$, velocity set-point $v_{C_1} \in [v_{\min}, v_{\max}]$, loiter radius $R_C > 0$, there exists $\gamma_1 \in \mathcal{K}_\infty$ such that the closed-loop system resulting from controlling the error system*

$$\dot{e}_1 = \begin{bmatrix} \frac{x}{R(x,y)} v \cos(e_{3,1} + \Psi_{C_1}) + \frac{y}{R(x,y)} v \sin(e_{3,1} + \Psi_{C_1}) \\ \frac{T_1 - D(v,\Phi_1)}{m} \\ \frac{g}{v} \tan \Phi_1 - \langle \nabla_z \Psi_{C_1}(z), f(z, \kappa_1(z)) \rangle \end{bmatrix},$$

with the controller

$$\begin{bmatrix} T_1 \\ \Phi_1 \end{bmatrix} = \kappa_1(x, y, v, \Psi, \Psi_{C_1}) := \begin{bmatrix} D(v, \Phi_1) - k_{T_1}(v - v_{C_1}) \\ \Phi_{C_1}(x, y, \Psi, \Psi_{C_1}) \end{bmatrix}, \tag{55}$$

where $k_{T_1} > 0$ and Ψ_{C1} is given in Eq. (40) and Φ_{C1} is given in Eq. (52), satisfies, for each $\epsilon > 0$,

1. $\langle \nabla V_1(e_1), \dot{e}_1 \rangle \leq -\gamma_1(|e_1|) + \epsilon$ *for all* $e_1 \in \mathbb{R}^3$ *such that* $[x\ y\ v\ \Psi]^\top \in \mathcal{C}_1$

where ζ is chosen such that

$$\frac{v_{max} d}{R_C} 2(R_C + d) |\sin \zeta| < \epsilon \tag{56}$$

In particular, an appropriate choice of γ_1 is

$$\gamma_1(s) = \min \left\{ \frac{v_{min} \beta R_C}{(R_C^2 + (R_C + d)^2)}, \frac{k_{T_1}}{m}, \chi \right\} s^2 \qquad \forall s \geq 0$$

C. Uniting Global and Local Controller

The process of uniting the global and local controllers into a hybrid controller is the process of defining the flow and jump sets for the hybrid controller. Following the framework in Sanfelice[5] and the construction in Example 3.23 therein, we design the parameters d and c determining the sets $\mathcal{C}_1, \mathcal{C}_2, \mathcal{D}_1$, and $\mathcal{D}_2$ in Eq. (20). So that

$$\mathcal{D}_2 \subset \mathcal{L}_{V_1}(c) \tag{57}$$

Since $\mathcal{C}_2$ is the closed complement of $\mathcal{D}_2$ for $q = 2$, we have that solutions from $\mathcal{C}_2$ approach $\mathcal{D}_2$ in finite time. In fact, $\mathcal{D}_2$ is given by the c-sublevel of $e_2 \mapsto V(e_2)$, which as established by Proposition 3, is globally attractive. From points z in $\mathcal{D}_2$, which due to Eq. (57) are also in $\mathcal{L}_{V_1}(c)$, we have that $R - R_c \leq \sqrt{2c}$. Hence, after a jump from $q = 2$ to $q = 1$, such points will be in $\mathcal{C}_1$ if

$$d > \sqrt{2c}$$

which is the constraint given in Eq. (22). Hence, we have

$$\mathcal{D}_2 \subset \mathcal{C}_1.$$

From points z in $\mathcal{C}_1$ we have that, according to Proposition 4, solutions are such that the error e_1 satisfies

$$V_1(e_1(t)) \leq \exp(-\bar{\alpha}(t - t_0)) V_1(e_1(t_0)) + (1 - \exp(-\bar{\alpha}(t - t_0)))\epsilon$$

over each interval of flow with $q = 1$, where $\bar{\alpha} = 2 \min \left\{ \frac{v_{min} \beta R_C}{(R_C^2 + (R_C + d)^2)}, \frac{k_{T_1}}{m}, \chi \right\}$. Hence, $V_1(e_1(t)) = \frac{1}{2}|e_1(t)|^2$ converges to $[0, \epsilon]$, and we have that

$$\lim_{t \to \infty} |e_1(t)| \leq \sqrt{2\epsilon}$$

as long as the solution stays in $\mathcal{C}_1$. To ensure this property, we pick

$$\sqrt{2\epsilon} < d$$

which guarantees that $|e_1| \leq \sqrt{2\epsilon}$ implies $|R - R_c| < d$, and hence the state z is in $\mathcal{C}_1$. The construction above provides the following properties when the parameters satisfy the conditions given earlier: we summarize as $d > \sqrt{2c}$, $\sqrt{2\epsilon} < d$, $c > \frac{1}{2}\left(\pi^2 + (v_{max} - v_{min})^2\right)$, $\nu > 0$, $\xi(s) > \frac{1}{2}$ if $|s| \geq \frac{\pi}{2}$ and $\xi(s) \geq 0$ if $|s| < \frac{\pi}{2}$, $\gamma(s) > \frac{1}{2}$ if $|s| \geq \frac{\pi}{2}$, and $\gamma(s) \geq 0$ if $|s| < \frac{\pi}{2}$, $\mu \in [0, 1]$, $k_{T_q} > 0$, $\chi > 0$, and $\zeta \in (0, \frac{\pi}{2})$ such that $\frac{v_{max} d}{R_C} 2(R_C + d)|\sin \zeta| < \epsilon$.

- For every point in $\mathcal{C}_2$ solutions approach $\mathcal{D}_2$, converge to it in finite time, and a switch to the local controller occurs.
- For every point in $\mathcal{C}_1$ solutions stay in $\mathcal{C}_1$ and the error e_1 approaches the set $\{e_1 : |e_1| \leq \sqrt{2\epsilon}\} \subset \mathcal{C}_1$.
- For every point in $\mathcal{D}_1$ or $\mathcal{D}_2$ away from $\mathcal{C}_1$ or $\mathcal{C}_2$ respectively, a jump switching q occurs.

Table 1. Simulation Parameters

UAV Parameter	Value	Units	Scenario Parameter	Value	Units	Gain	Value
W	24525	N	μ	0.1	-	ξ	see Eq. (58)
C_{Lmax}	0.85	-	V_{C_1}	160	$\frac{m}{s}$	k_{T_1}	1000
C_{D0}	0.002	-	V_{C_2}	200	$\frac{m}{s}$	k_{T_2}	1000
K	59	-	ρ	1.112	$\frac{kg}{m^3}$	ζ	0.1745
S_{ref}	35.15	m^2	g	9.81	$\frac{m}{s^2}$	γ	see Eq. (59)
T [min max]	[50 9000]	N				χ	10
						ν	10

IV. Numerical Analysis

The hybrid system for the UAV transition between transit and loiter was implemented in a Simulink model[15] to further explore and verify the analytical results presented. A well designed hybrid control system will switch between the transit and loiter modes in such a way that minimizes transit time without overshooting the loiter area. The inputs and gains used for the presented simulation results are listed below in Table 1.

Several of the gain parameters listed in the table vary as a function of the vehicle's flight conditions while still satisfying the constraints established in the control law analysis. The criteria for varying the gains is listed below.

$$\xi = \frac{3}{2\pi}|\Delta_2|. \tag{58}$$

$$\gamma = \frac{3}{2\pi}|\Delta_1|. \tag{59}$$

The local/global switching criteria for the simulation were set as

$$c = \frac{1}{2}(\pi^2 + (v_{max} - v_{min})^2) + 1 \tag{60}$$

$$d = \sqrt{2c} + 200 \tag{61}$$

where Eq. (60) and Eq. (61) were selected to satisfy Eq. (21) and Eq. (22) respectively. Simulation results are shown to demonstrate performance of the algorithm.

A. Outside the Loiter Circle (Disk)

For the scenario starting outside the loiter circle a loiter radius (R_C) of 350 m was used. Figure 6 shows a performance time history for the trajectory. The vehicle is initially headed in the wrong direction, but the global controller reverses heading to fly towards the center of the loiter circle. The hysteresis between $\mathcal{C}_1$ and $\mathcal{C}_2$ prevents chatter between the local and global controllers. The vehicle switches from the global controller to the local controller at a point inside the local controller flow set and follows a trajectory that approaches the loiter circle on a tangent and ultimately tracks the loiter circle. The switch from the global controller to the local controller occurs at approximately 7 seconds. In

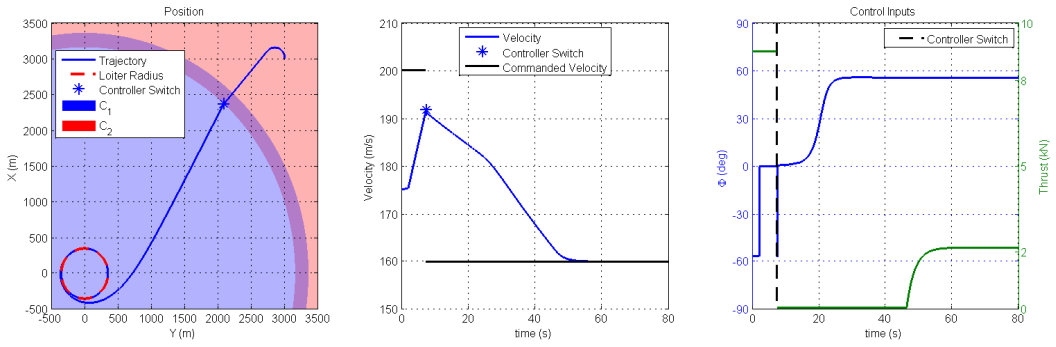

Figure 6. Simulation results starting outside the loiter circle

the global control region, the vehicle attempts to accelerate to the commanded global controller velocity. For the first

two seconds the vehicle does not accelerate quickly because of the high drag while turning. Once the vehicle has completed its turn it accelerates more quickly to the global commanded velocity until the switch to the local controller. In the local control region, the thrust is commanded to its minimum while the vehicle decelerates to the commanded loiter velocity. The simulation results confirm that the controller design provides the desired performance within each of the local and global modes. Also, the design of the local and global sets prevents chatter between the two modes.

V. Conclusion

A hybrid control system for UAV waypoint loitering was analyzed and demonstrated. Asymptotic stability was established, and verified by simulation, for the UAV system modeled in a plane with thrust and bank angle as control inputs. There are several opportunities for future work. One could be to expand the control algorithm to be three dimensions by including altitude and account for time varying mass. Another possibility could be to expand the algorithm to use other modes such as changing altitude. Though this paper focused on a UAV as the system being controlled, the algorithm could be applied to other systems such as boats or wheeled vehicles.

VI. Acknowledgment

Many thanks to our families for patiently giving up evenings and weekends to let us work on this project. Research by R. G. Sanfelice was partially supported by NSF Grants no. ECS-1150306 and CNS-1544396, and by AFOSR Grants no. FA9550-12-1-0366 and FA9550-16-1-0015.

References

[1]E. Frew, D. Lawrence, C. D. J. E. and Pisano, W., "Lyapunov Guidance Vector Fields for Unmanned Aircraft Applications," *IEEE*, Vol. 27, No. 2, 2007, pp. 194–204, also AIAA Paper 89–0269, Jan. 1989.

[2]D. Lawrence, E. F. and Pisano, W., "Lyapunov Vector Fields for Autonomous Unmanned Flight Control," *AIAA*, Vol. 31, No. 5, 2008, pp. 1220–1229.

[3]S. Park, J. D. and How, J., "A New Nonlinear Guidance Logic for Trajectory Tracking," *AIAA*, 2004.

[4]Prieur, C., "Uniting local and global controllers with robustness to vanishing noise," *Math. Control Signals Systems*, Vol. 14, 2001, pp. 143–172.

[5]Goebel, R., Sanfelice, R. G., and Teel, A. R., *Hybrid Dynamical Systems: Modeling, Stability, and Robustness*, Princeton University Press, 2012.

[6]Prieur, C., Goebel, R., and Teel, A. R., "Hybrid feedback control and robust stabilization of nonlinear systems," Vol. 52, No. 11, November 2007, pp. 2103–2117.

[7]Sanfelice, R. G., Teel, A. R., and Goebel, R., "Supervising a family of hybrid controllers for robust global asymptotic stabilization," *Proc. 47th IEEE Conference on Decision and Control*, Cancun, Mexico, 2008, pp. 4700–4705.

[8]Sanfelice, R. G. and Teel, A. R., "A "throw-and-catch" hybrid control strategy for robust global stabilization of nonlinear systems," *Proc. 26th American Control Conference*, New York, NY, 2007, pp. 3470–3475.

[9]Efimov, D., A., A. L., and Panteley, E., "Robust output stabilization: Improving performance via supervisory control," *International Journal of Robust and Nonlinear Control*, Vol. 21, No. 10, 2011, pp. 1219–1236.

[10]Jung, D. and Tsiotras, P., "Bank-to-Turn Control for a Small UAV using Backstepping and Parameter Adaptation," *Georgia Tech*, 2008.

[11]Witkowska, A. and 'Smierzchalski, R., "Nonlinear Backstepping Ship Course Controller," *International Journal of Automation and Computing*, 2009.

[12]M. Krstic, I. K. and Kokotovic, P., *Nonlinear and Adaptive Control Design*, Wiley-Interscience, New York, 3rd ed., 1995.

[13]Khalil, H., *Nonlinear Systems*, Prentice Hall, 3rd ed., 2002.

[14]Raymer, D., *Aircraft Design: A Conceptual Approach*, American Institute of Aeronautics and Astronautics Inc., 4th ed., 2006.

[15]R. G. Sanfelice, D. A. Copp, . P. N., A Toolbox for Simulation of Hybrid Systems in Matlab/Simulink: Hybrid Equations (HyEQ) Toolbox, Proceedings of Hybrid Systems: Computation and Control Conference, Aug. 2013.